Clays and Clay Minerals, Vol. 62, No. 2, 89–101, 2014.

TEMPERATURE EFFECTS ON THE CRYSTALLINITY OF SYNTHETIC NONTRONITE AND IMPLICATIONS FOR NONTRONITE FORMATION IN COLUMBIA RIVER BASALTS

LESLIE L. BAKER[1,2,*] AND DANIEL G. STRAWN[2]

[1] Department of Geological Sciences, University of Idaho, Moscow, ID 83844-3022, USA
[2] Department of Plant, Soil, and Entomological Sciences, University of Idaho, Moscow, ID 83844-2339, USA

Abstract—The formation conditions of the ferric smectite nontronite are not fully understood. The present study couples experimental and analytical data with field observations in an attempt to constrain the rate and temperature of formation of naturally occurring nontronites from Columbia River Basalt flows. Synthetic Fe-Al-Si gels were incubated at temperatures ranging from 4 to 150ºC for 4 weeks. Samples were analyzed using Fe K-edge X-ray fluorescence spectroscopy (XAFS). Spectra of the synthesized nontronites were compared with spectra of natural samples collected from weathered Columbia River Basalt flows. Cation ordering in the synthetic samples increased with incubation temperature, but the synthetic clays did not approach the degree of crystal ordering of the natural nontronite samples. These observations suggest that highly ordered natural nontronites require longer crystallization times than are typically used in laboratory experiments. The natural samples were found filling open cracks near flow surfaces, indicating that the clays formed at temperatures below the boiling point of water. A comparison of experimental and field timescales with other estimates of nontronite growth rates suggests that natural nontronite crystallization in the region must have occurred at ambient, near-surface temperatures over timescales of up to millions of years.

Key Words—Columbia River Basalts, Fe K-edge XAFS, Nontronite.

INTRODUCTION

Nontronite is a dioctahedral ferric smectite with an ideal mineral formula of $Na_{0.4}Si_{3.6}Al_{0.4}Fe_2O_{10}(OH)_2$. In nature it is most commonly found as a weathering product of mafic volcanic rocks such as basalt (Allen and Scheid, 1946; Benson and Teague, 1982; Jakobsson and Moore, 1986; Meunier *et al.*, 2008), but is also observed in metamorphic rocks (Eggleton, 1977; Keeling *et al.*, 2000) and in sediments associated with seafloor hydrothermal vents (Cole and Shaw, 1983; Köhler *et al.*, 1994; Ueshima and Tazaki, 2001; Severmann *et al.*, 2004; Dekov *et al.*, 2007). Nontronite has been identified as a potentially important phase on Mars, where its presence in deep canyons provides direct evidence for aqueous alteration of Martian crustal rocks in the ancient past (Bishop *et al.*, 2008; Ehlmann *et al.*, 2011). Natural nontronites range from nearly pure Fe endmember phases to mixed Fe-Al phases that are sometimes described as ferruginous smectites. Whatever their composition, most well studied natural nontronites are comparable to one another in terms of their crystallinity (Allen and Scheid, 1946; Manceau *et al.*, 1998; Gates *et al.*, 2002). Although nontronite occurrence and properties are well documented, the formation conditions of this clay mineral are not well understood.

To study nontronite formation and properties, the mineral has been synthesized in the laboratory using various methods. Ferric smectites were synthesized (Harder, 1976, 1978) by aging co-precipitates of ferrous hydroxides and silica at 3−22ºC. The formation of ferric smectites was observed only (Harder, 1976, 1978) from starting products containing Fe(II) and aged in the presence of sodium dithionite, a reductant. Under these conditions, synthetic products that had XRD peaks indicative of clay minerals after synthesis times as short as 2 weeks were described, although the clays were described as being very poorly crystalline. Harder (1976, 1978) also noted that the formation of Fe-rich clay minerals was promoted by synthesis at pH > 7, and that nontronite formed in solutions with Fe:Si between 1:10 and 1:3. These synthesis conditions are similar to conditions observed for nontronite formation in seafloor hydrothermal sediments, where ferric hydroxide-silica co-precipitates recrystallize to nontronite (Cole and Shaw, 1983; Köhler *et al.*, 1994; Ueshima and Tazaki, 2001; Severmann *et al.*, 2004).

Aluminous nontronites were also synthesized by Farmer *et al.* (1991, 1994) at 23 and 89ºC and pH 8, from solutions of $AlCl_3$, $FeCl_2$, and silicic acid. Those authors obtained poorly ordered, hisingerite-like materials at the lower temperature, but at the higher temperature, ordered nontronitic layer silicates were

* E-mail address of corresponding author:
lbaker@uidaho.edu
DOI: 10.1346/CCMN.2014.0620202

formed after 8 weeks. Natural nontronites were proposed by Farmer *et al*. (1991, 1994) to form by initial precipitation of a trioctahedral Fe(II) silicate, which transforms to dioctahedral nontronite through oxidation of Fe and ejection of excess octahedral cations, but they noted that crystallization in their experimental systems occurred primarily after oxidation of Fe(II) to Fe(III).

Synthesis of ferric smectites from gels under reducing and oxidizing conditions, were investigated by Decarreau and Bonnin (1986) and Decarreau *et al.* (1987), respectively. In contrast to the results of Harder (1976, 1978), those authors observed growth of ferric smectites only under oxidizing conditions. Decarreau and colleagues also observed smectite growth to be very slow except at elevated temperatures. From measurements of crystal growth at several temperatures, they derived an Arrhenius relationship for nontronite formation, indicating that a ferric smectite with coherent domains ~100 Å in size should form in ~10 y at 25ºC and in ~200 years at 2ºC. Decarreau *et al.* (2008) extended these methods to synthesize high-charge Fe-endmember nontronites. Clays synthesized by those authors displayed a high level of tetrahedral Fe substitution, estimated at 30% of total Fe. The crystallinity of the synthetic nontronites increased with increasing temperature up to 150ºC, above which aegirine ($NaFeSi_2O_6$) formed rather than nontronite.

Previous experimental studies on nontronite synthesis have provided insight into conditions required for nontronite formation, but many questions remain. Application of these studies to nontronite formation from mafic precursors suggests that the formation of highly crystalline nontronites in nature may require long formation times at relatively low temperatures. The present study further investigated this hypothesis by examining the crystallinity of a set of synthetic nontronites incubated at 23, 95, and 150ºC. Poorly crystalline phases are often difficult to study using techniques such as XRD. In the present study, synthetic nontronites were analyzed using Fe K-edge XANES and EXAFS methods, which provide information on the shells of atoms immediately surrounding a central iron atom and, therefore, allow for insights into the molecular structure of nontronite samples that have limited (XRD-amorphous) structure. The XAFS spectra from synthetic samples were compared to spectra of natural nontronite samples formed by weathering of Columbia River Basalts (CRB). These data on the relative crystallinities of the synthetic and natural samples, coupled with field constraints on natural nontronite occurrences, help to constrain the physical parameters of nontronite formation by basalt weathering.

METHODS

Natural and synthetic sample acquisition/preparation

A single batch of nontronite precursor gel was synthesized using a method modified from the nontronite-synthesis procedures of Farmer *et al.* (1994) and Decarreau and Bonnin (1986), and the allophane-synthesis procedure of Montarges-Pelletier *et al.* (2005). This gel had an Fe:Al molar ratio of 1:1 and a Si:(Fe,Al) molar ratio of 3:1. To synthesize the precursor material, 0.1 M $Fe(NO_3)_2$ and 0.1 M $Al(NO_3)_3$ were mixed with tetraethyl orthosilicate and one drop of hydrazine, and stirred rapidly on a magnetic stir plate. A solution of 0.1 M NaOH was titrated into the solution at a rate of 1 mL min^{-1} under rapid stirring, forming a dark blue-green gel. The final pH of this gel suspension was 7.6 after titration. The suspension was adjusted to pH 12.25 with 1 M NaOH. The gel was then separated into aliquots for further incubation at different temperatures.

All samples were incubated for a period of 28 days. One aliquot of the initial gel (nontronite 1) was washed twice in deionized water and stored under refrigeration at 4ºC, and remained a dark green gel. A second aliquot (nontronite 2) was incubated under stirring at room temperature (23ºC); the final product was a suspension of brown gel with a final pH of 11.37. A third aliquot (nontronite 3) was incubated at 95ºC on a temperature-controlled stirring hot plate and turned to a thick, tan suspension with a final pH of 10.64. A fourth aliquot (nontronite 4) was incubated at 150ºC in a Teflon cup inside a stainless steel bolted-closure autoclave in the presence of liquid water, and remained a dark blue-green color; its final pH was not measured. At the end of the 28-day incubation period, all samples were stored under refrigeration. A small amount of each synthetic nontronite was dried for analysis. The dried synthetic nontronites were all light tan in color.

Naturally occurring nontronitic clays were collected near the towns of Garfield and Trinidad in the state of Washington, USA. These sites were the original collection localities for the widely used but now commercially unavailable reference standards, Garfield nontronite (API#33a, formerly available from Wards Natural Science, Rochester, New York, USA) and SWa-1 ferruginous smectite (formerly available from the Source Clays Repository of The Clay Minerals Society). Nontronite from Garfield was collected from the sampling location described by Kerr and Kulp (1949). Green, waxy nontronite was found filling narrow (~1 cm) cracks in the Priest Rapids Member of the Wanapum Basalt of the Columbia River Basalt Group (Reidel *et al.*, 2013). This is the capping basalt in this locality and the nontronite-filled cracks were located within 1 m of the basalt surface. This sample is designated as UI-Garfield here to distinguish it from the original Garfield nontronite.

The site at Trinidad, from which the original SWa-1 sample was collected, is located on Washington State Highway 28 just east of the town of Trinidad and was described in the field notes and maps of J.A. Kittrick that are archived in the Department of Crop and Soil Sciences, Washington State University and available

https://doi.org/10.1346/CCMN.2014.0620202 Published online by Cambridge University Press

from the journal's data depository: www.clays.org/JOURNAL/JournalDeposits.html. The nontronite at this locality formed at the contact between a basalt flow of the Frenchman Springs Member of the Wanapum Basalt of the Columbia River Basalt Group and an underlying paleosol developed on underlying Grand Ronde Basalt (Reidel *et al.*, 2013). The Frenchman Springs flow is the capping basalt at this locality, and green, powdery clays were found filling void spaces and coating altered basalt fragments located ~2 m beneath the flow surface.

Once collected, the nontronite samples were crushed gently by hand using an agate mortar and pestle and suspended in deionized water, and the very fine clay fraction (<0.05 μm) was separated by centrifugation. The separated clay fraction was analyzed as described below, without further purification.

Laboratory analyses

The dried nontronite samples were analyzed using diffuse reflectance Fourier-transform infrared spectroscopy (FTIR) and powder X-ray diffractometry (XRD). The FTIR analyses were carried out on a Perkin-Elmer System 2000 (Thermo Scientific, Waltham, Massachusetts, USA), using a mixture of 3 wt.% nontronite in optical-grade KBr. Spectra were processed using the Kubelka-Munk algorithm provided in the Perkin Elmer *Spectrum* 2.0 software (Thermo Scientific, Waltham, Massachusetts, USA). The XRD scans were run on a Siemens D5000 diffractometer (Bruker AXS, Karlsruhe, Germany) and data were analyzed using the *Diffracplus Eva* evaluation program (Bruker AXS, Karlsruhe, Germany). Natural clay samples were fused with lithium metaborate and analyzed on a Thermo Electron iCAP inductively coupled plasma spectrometer (ICP-AES) (Thermo Scientific, Waltham, Massachusetts, USA) for bulk composition (results are shown in Table 1).

Bulk Fe K-edge XAFS data for synthetic and natural nontronite samples were collected on Beamline 7-3 of the Stanford Synchrotron Radiation Laboratory (SSRL). The monochromator for this beamline consisted of two parallel Si(220) crystals with a 6-mm entrance slit. All samples were run in a liquid He-cooled cryostat at a temperature of 7 K. Fluorescence data were collected using a PIPS detector. Step size through the XANES region was 0.35 eV. Powdered samples were smeared on filter paper, which was cut into strips, stacked three layers thick, and sealed in the sample holder with Kapton tape. The synthetic nontronites incubated at 95 and 23ºC were analyzed as gels, which were packed into the sample holder in a layer of uniform thickness and sealed with Kapton tape. Both transmission and fluorescence spectra were collected for all samples; fluorescence spectra were used for all samples because of their higher signal to noise ratio, but the two datasets were comparable and fluorescence data did not show any self-absorption artifacts.

One to three XAFS scans per sample were calibrated to Fe foil and averaged using the program *SixPack* (Webb, 2005). Processing and shell fitting were carried out using the programs *Athena* and *Artemis* (Ravel and Newville, 2005). Raw and normalized intensity data were exported into the plotting program *Origin* 8.6 (OriginLab, Northampton, Massachusetts, USA). Pre-edge peaks were fitted in *Origin*; a spline was fitted to each baseline between 7110 and 7120 eV and subtracted, after which peak locations were identified and peak heights were measured.

Shell fitting of the XAFS spectra was carried out using the 6-shell model described by Baker and Strawn (2012), as modified from a nontronite model described by Manceau *et al.* (1998). The model parameters are given in Table 2. All parameters were set, and fitting was carried out, as described for UI-Garfield nontronite in Baker and Strawn (2012). Briefly, fitting was carried out using backscattering paths to first-shell oxygen, Fe, and Al in the octahedral sheet and six associated oxygen atoms (O3), and Si in the tetrahedral sheet and two associated O atoms (O2). All backscattering path lengths were optimized. To account for possible non-random distribution of octahedral cations, the Fe-Fe and Fe-Al backscattering paths were weighted with parameters that were constrained to sum to three (*e.g.* three total neighboring octahedral cations), and this parameter value was optimized (*N*Fe; Table 2). Debye-Waller parameters were optimized for the first shell and the outer O shells (O2 and O3 paths), and fixed for the octahedral and tetrahedral cation backscattering paths, as

Table 1. Sample compositions of two natural nontronites (purified clay separates) and nominal (as synthesized) composition of synthetic nontronite. Oxide contents are given in weight percent.

	SiO_2	Al_2O_3	Fe_2O_3	MgO	CaO
UI-Garfield	56.3	5.35	35.64	1.39	0.57
Trinidad	57.2	5.39	34.26	1.47	1.69
Nominal synthetic	57.9	16.39	25.67	0	0
Standard Garfield*	51.7	7.54	36.43	0.16	3.52
Standard SWa-1*	56.7	11.04	26.65	1.302	3.16

* from Gates *et al.* (2002).

https://doi.org/10.1346/CCMN.2014.0620202 Published online by Cambridge University Press

Table 2. Theoretical paths, coordination numbers, and path lengths for smectite used for shell modeling generated using *Feff*, as described by Baker and Strawn (2012). In fitting, Fe and Al coordination numbers were optimized, but constrained to sum to a total of 3 octahedral cations (*N*Fe is the number of Fe atoms in the structure, less than or equal to three).

Path	CN	R (Å)
Fe−O1	6	1.96−2.04
Fe−Fe1	*N*Fe	3.05
Fe−Al1	3−*N*Fe	3.05
Fe−Si	4	3.26
Fe−O2	2	3.45
Fe−O3	6	3.74−3.82

shown in Table 3.

ANALYTICAL RESULTS

Bulk analyses

Bulk chemical analyses for the UI-Garfield and Trinidad samples (Table 1) revealed compositions typical of nontronites, but different from published analyses of the standard samples from those localities. The analyzed composition of the Trinidad nontronite contained less Al_2O_3 and more Fe_2O_3 than published analyses of the SWa-1 standard that was collected from the same site. The analyzed composition of UI-Garfield nontronite contained more SiO_2, more MgO, and less Al_2O_3 than published analyses of the commercial Garfield nontronite standard. These differences may result from varying composition of the nontronite itself; although the samples in this study were collected from the same outcrops as the standard clays, specific collection sites (individual veins) were unknown and probably differed. Some compositional differences could potentially also result from differences in sample preparation. In this study, as in the study by Gates *et al.* (2002), very fine clay separates were physically separated for analysis in an effort to remove all Fe (oxyhydr)oxides. A slight excess of analyzed SiO_2 in the natural samples (Table 1) may indicate the presence of minor opaline silica. The synthetic nontronites were not analyzed independently due to the small quantity of material available; the composition shown for these samples in Table 1 is the nominal composition expected from the synthesis. As a result of the solution compositions used to synthesize the precursor gels, Na is expected to be the only interlayer cation present.

XRD

The XRD data (Figure 1) showed that none of the synthetic nontronites had achieved the crystallinity of the natural UI-Garfield nontronite sample. The synthetic nontronite incubated at 150ºC displayed reflections at *d* spacings typical of nontronite, with the 001 reflection at 11.8 Å, a peak at 3.8 Å, and inflections at 2.7 and 2.2 Å. These peaks were much less well defined than in the UI-Garfield nontronite. The synthetic nontronite incubated at 95ºC showed little XRD-detectable structure; a minor inflection at the 001 band at 11.8 Å and another at 3.8 Å were present, but much of this material appeared to be amorphous at the scale sensed by XRD. This material appeared to be less crystalline than the nontronite synthesized by Decarreau *et al.* (2008) at 90ºC, and more comparable to their 75ºC sample. No structure was detectable by XRD in the lower-temperature samples (not shown).

FTIR

In agreement with XRD analyses, FTIR data (Figure 2) also showed that none of the synthetic nontronites approached the structural development of either UI-Garfield or Trinidad nontronite. The UI-Garfield sample displayed typical nontronite IR peaks including the Fe–Fe–OH-stretching peak at 3565 cm^{-1}, the main Fe−Si−O stretch near 1005 cm^{-1}, Fe−Fe−OH

Table 3. Fitting results for nontronite samples. All path lengths were optimized independently unless otherwise noted; other variables optimized in fitting are annotated.

Path	UI-Garfield E0 = −1.98 R-factor = 0.025			Trinidad E0 = −1.16 R-factor = 0.024			150ºC synthetic E0 = −3.46 R-factor = 0.015			95ºC synthetic E0 = −3.66 R-factor = 0.012			23ºC synthetic E0 = −4.63 R-factor = 0.027		
	CN	*R* (Å)	σ^2 (Å^2)	CN	*R* (Å)	σ^2 (Å^2)	CN	*R* (Å)	σ^2 (Å^2)	CN	*R* (Å)	σ^2 (Å^2)	CN	*R* (Å)	σ^2 (Å^2)
Fe−O1	6	2.00	0.006[a]	6	2.00	0.006[a]	6	1.99	0.009[a]	6	1.97	0.009[a]	6	1.96	0.012[a]
Fe−Fe1	3	3.08	0.005	2.48[a]	3.07	0.005	2.05[a]	3.05	0.005	1.66[a]	3.04	0.005	0.88[a]	2.88	0.005
Fe−Al1	0	–	–	0.52[a]	3.01	0.005	0.95[a]	3.05	0.005	1.34[a]	3.03	0.005	2.12[a]	2.92	0.005
Fe−Si1	4	3.23	0.005	4	3.24	0.005	4	3.26	0.005	4	3.26	0.005	4	3.23	0.005
Fe−O2	2	3.42	0.008[b]	2	3.33	0.009[b]	2	3.45	0.008[b]	2	3.46	0.028[b]	2	3.23	0.010[b]
Fe−O3	6	3.80	0.008[b]	6	3.80	0.009[b]	6	3.74	0.008[b]	6	3.81	0.028[b]	6	3.59	0.010[b]

[a] Values optimized in fitting
[b] Values optimized in fitting, but constrained to be equal to one another.

https://doi.org/10.1346/CCMN.2014.0620202 Published online by Cambridge University Press

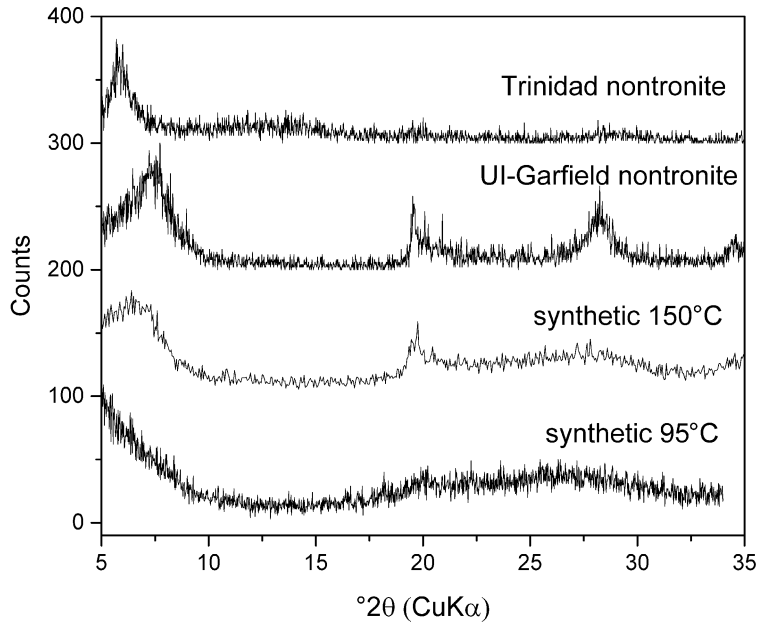

Figure 1. Bulk-powder XRD patterns of UI-Garfield and Trinidad nontronites, and of nontronites synthesized at 95 and 150ºC. Nontronites synthesized at lower temperatures showed no identifiable XRD peaks.

bending feature at 818 cm^{-1}, and Si–O–Fe bending vibration at 675 cm^{-1} (Frost *et al.*, 2002; Gates, 2005). In Fe-substituted smectites, an Fe–Al–OH stretching peak is observed at 3590 cm^{-1} (Frost *et al.*, 2002), and an Fe–Al–OH bend that is present at 890 cm^{-1} in higher-Al clays shifts to 870 cm^{-1} with increasing Fe content (Russell and Fraser, 1994). The latter band was observed in the spectrum of the Trinidad nontronite, but not in the spectrum of the UI-Garfield nontronite (Figure 2). Because the two clay samples had similar bulk composition (Table 1), this suggests a difference in cation ordering between them, with more Fe-Al nearest neighbors being present in Trinidad nontronite than in UI-Garfield nontronite. A band at 844 cm^{-1} was also observed in UI-Garfield nontronite; the presence of this band in combination with the 818 cm^{-1} band is considered diagnostic of nontronite (Gates, 2005; Gates, 2008). This band may arise from Fe-Fe–OH

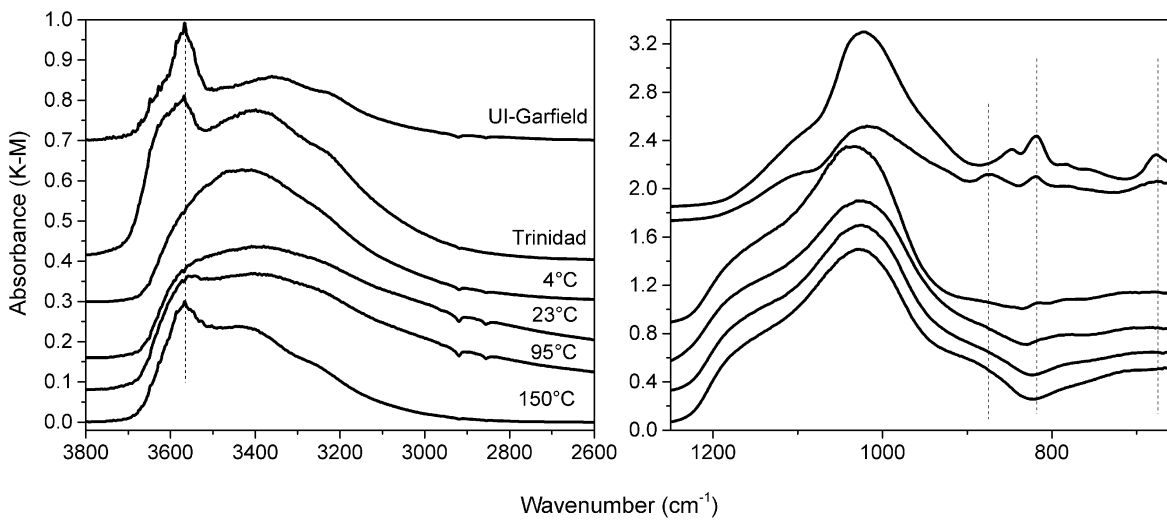

Figure 2. IR spectra of UI-Garfield nontronite and of nontronites crystallized at the temperatures indicated. The locations of characteristic nontronite peaks are indicated by dotted lines at 3565 cm^{-1} (Fe-Fe-OH-stretch), 870 cm^{-1} (Fe–Al–OH bend), 818 cm^{-1} (Fe–Fe–OH bend), and 675 cm^{-1} (Fe–O out of plane vibration). The shoulder near 1100 cm^{-1} in the UI-Garfield and Trinidad samples suggests the presence of amorphous or opaline silica in the sample (Shoji *et al.*, 1993).

https://doi.org/10.1346/CCMN.2014.0620202 Published online by Cambridge University Press

bending, like the feature at 818 cm^{-1} (Frost *et al.*, 2002), perhaps due to splitting as a result of tetrahedral Fe substitution (Gates, 2008). A number of the characteristic spectral bands of nontronite or ferruginous smectites are shifted by the presence of Fe(II) in the structure (Neumann *et al.*, 2011). No such characteristic shifts were observed for the synthetic nontronites in the present study, in spite of evidence (discussed below) for some Fe(II) in the sample incubated at 150ºC. A broad shoulder centered near 1100 cm^{-1} in both the UI-Garfield and Trinidad samples suggested the presence of some amorphous or opaline silica (Shoji *et al.*, 1993), in agreement with the high SiO_2 measured for these samples. Opal is a common weathering product of Columbia River Basalts and macroscopic opal deposits were observed at the Trinidad field site, although not at the Garfield site.

The FTIR spectrum of the nontronite incubated at 150ºC was very similar to that of the 150ºC synthetic nontronite of Decarreau *et al.* (1987). Inflections at 844 and 818 cm^{-1} correspond to Fe–Fe–OH bending that are characteristic of nontronite (Gates, 2005; Gates, 2008). A band at 870 cm^{-1} suggests Fe–Al–OH bending, as would be expected for this high-Al composition. All the peaks in the 150ºC sample were weaker and broader than those observed in the natural nontronite samples, indicating a lower overall degree of crystallinity. The broadening and eventual disappearance of characteristic spectral lines in the nontronites synthesized at lower temperatures suggest that they were less crystalline than the nontronites synthesized at higher temperatures. The 95ºC nontronite displayed only a poorly developed Fe–Fe–OH stretching peak at ~3555 cm^{-1}, and an Fe–Si–O stretching peak near 1025 cm^{-1}. The Fe–Si–O stretch was the only one well developed in lower-temperature sample spectra. All the synthetic samples displayed a broad, very weak inflection near 870 cm^{-1} that may have arisen from Fe–Al–OH bending.

XANES pre-edge

The XANES spectra of natural nontronites were very similar to one another (Figure 3), except for a split pre-edge peak in the UI-Garfield nontronite that was not observed for the Trinidad nontronite. This peak splitting is typical of octahedrally coordinated high-spin Fe(III) in a relatively undistorted environment (Westre *et al.*, 1997). The amplitude and shape of the Fe K-edge XANES pre-edge peak arise from the local symmetry environment around the central Fe atom, which is influenced both by the presence of tetrahedrally coordinated Fe and by isomorphic substitution of other cations such as Al- or Mg-for-Fe in surrounding sites. According to Gates *et al.* (2002), the SWa-1 standard nontronite (from the same site as the Trinidad sample) contains no tetrahedral Fe. The Trinidad nontronite had similar Al and Mg content as the UI-Garfield nontronite (Table 1) although, as discussed above, its IR spectrum indicated more Fe–Al–O bonding (Figure 2). The increased distortion around the central Fe atom in the Trinidad sample indicated by the unsplit pre-edge peak may be explained by a difference in cation ordering between this sample and the UI-Garfield sample.

The pre-edge peaks in the XANES spectra of synthetic nontronites are not split. In addition, the peak amplitudes of the pre-edge peak in nontronites synthesized at 95ºC and 23ºC were greater than that in the sample synthesized at 150ºC. As with the Trinidad nontronite, the high Al content of the synthetic samples may account for the absence of splitting in the pre-edge

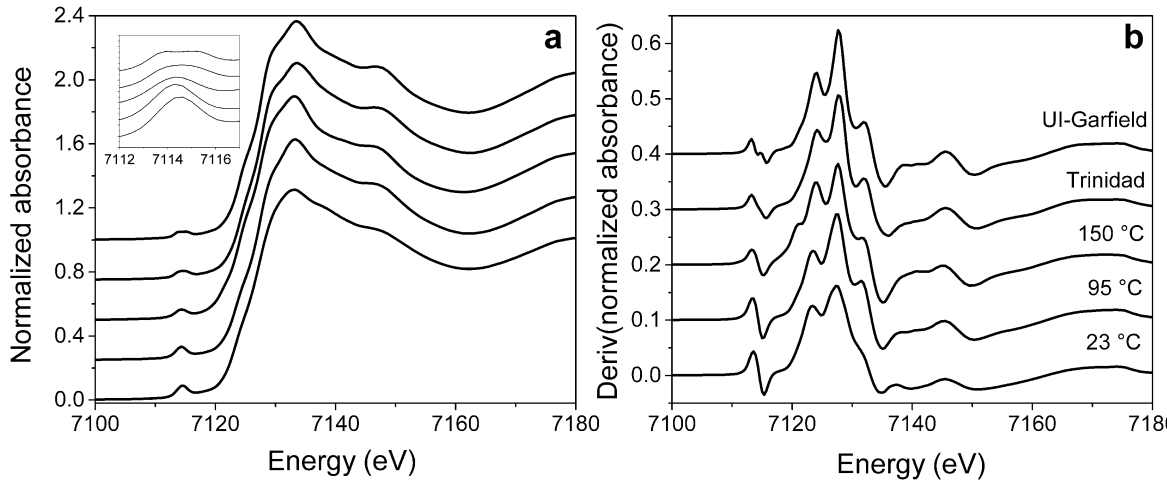

Figure 3. Normalized (a) and first-derivative (b) XANES spectra of UI-Garfield and Trinidad nontronites, and of synthetic nontronites crystallized at 23, 95, and 150ºC. The inset in (a) shows the pre-edge region of the XANES spectrum. The arrow in (b) indicates a low-energy shoulder on the synthetic 150ºC sample discussed in the text. Spectra are offset for clarity. The sample incubated at 4ºC is not shown, but is identical to that at 23ºC.

https://doi.org/10.1346/CCMN.2014.0620202 Published online by Cambridge University Press

peaks. The increased pre-edge peak amplitude of the lower-temperature samples may result from the presence of tetrahedrally coordinated Fe (Westre *et al.*, 1997), or from distortion due to a high octahedral Al content (Manceau *et al.*, 1990).

These explanations can be evaluated by examining Fourier-filtered first-shell spectra. Detection limits for tetrahedral Fe are ~3% of total Fe (Manceau *et al.*, 1990; Gates *et al.*, 2002). If tetrahedral Fe is present, the first-shell spectrum will include contributions from the shorter Fe−O bonds in tetrahedral complexes, and the backscattered wave will be out of phase with waves from Fe in purely octahedral coordination, creating a slight shift in the peak positions. Back-transformed spectra of the 95ºC and 23ºC synthetic nontronites (Figure 4) were shifted slightly at high energy relative to spectra of the Trinidad and UI-Garfield nontronites, which do not contain significant tetrahedral Fe (Gates *et al.*, 2002). This suggests that some tetrahedral Fe was present in the lower-temperature synthetic nontronites. The filtered spectrum of the 150ºC synthetic nontronite was in phase with the Trinidad and UI-Garfield nontronite spectra, suggesting that little tetrahedral Fe is present in this sample. These observations suggest that the increased amplitude of the XANES pre-edge peaks for the low-temperature nontronite samples results from the presence of tetrahedrally coordinated Fe in these samples. However, the high Al content of the synthetic samples is probably contributing to their pre-edge peak amplitudes also.

XANES

The main-edge XANES spectra of the synthetic nontronites were similar to those of natural nontronites from Garfield and Trinidad. The 150ºC sample had an extra edge inflection at 7120 eV (arrow in Figure 3b) that was not present in the natural samples or in the other synthetic samples. This inflection suggests the presence of Fe(II) in the 150ºC sample. Unlike the other synthetic samples, which were incubated in air, this sample was incubated in a sealed, unbuffered, stainless-steel pressure vessel. Thus, the presence of Fe(II) suggests that Fe was not completely converted to Fe(III) during incubation under these oxygen-limited conditions. The small size of the inflection feature, however, suggests that the proportion of Fe(II) in this sample is minimal, which is further supported by the overall resemblance of this spectrum to the spectra of the natural nontronites that do not contain Fe(II).

The XANES spectra of Fe-bearing clay minerals (Baker *et al.*, 2010) and of Fe-substituted allophanes (Baker and Strawn, 2012) typically display an inflection at 7132 eV, most easily observed in the first-derivative spectrum. This inflection was also present in the spectra of the synthetic nontronites, although relatively poorly developed in the synthetic nontronite incubated at 23ºC.

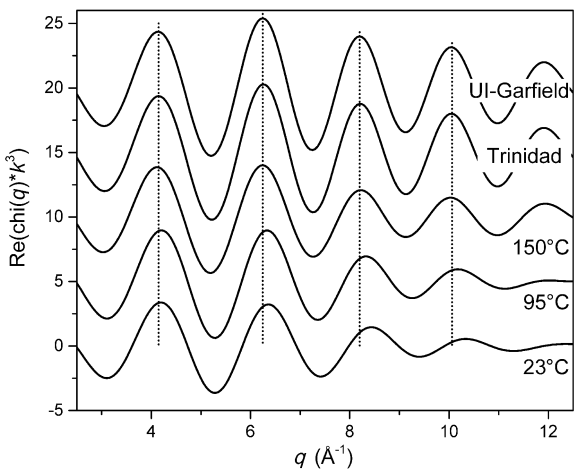

Figure 4. Back-transformed spectra of a first-shell backscattering peak ($\Delta R = 1-2$ Å) in UI-Garfield and Trinidad nontronites, and of synthetic nontronites crystallized at 23, 95, and 150ºC. The sample incubated at 4ºC is not shown, but is identical to that at 23ºC. Vertical dotted lines indicate peak positions for comparison.

EXAFS

The EXAFS spectra of natural nontronite samples (Figure 5) displayed many similarities to one another. The Fe−O backscattering peaks located near 2 Å in the Fourier-transformed spectra (Figure 5b) had similar magnitudes, in agreement with the bulk analyses, indicating that the two clay samples have similar octahedral cation compositions (Table 1). The second peak near 3 Å in the Fourier-transform results from backscattering from the three nearest-neighbor cations, and the peak at 4.8 Å results from backscattering by six second-octahedral neighboring Fe cations (Manceau *et al.*, 1998); both these peaks had lower amplitude for the Trinidad sample than for the UI-Garfield sample. This observation supports the suggestion above that the two nontronite samples, although having very similar bulk composition, may exhibit different cation ordering within their octahedral sheets. Small inflections and shoulders in the chi spectra of the natural samples (Figure 5a), such as those near 4, 6, 7.5, 9, and 11 $Å^{-1}$, were slightly different in the two samples, suggesting some minor differences between the two clays. Many of these inflections in the chi spectra result from backscattering by relatively distant atoms, or from multiple scattering (Manceau *et al.*, 1998). Back transformation of the Fourier-transformed spectra to exclude backscatterers beyond 4.5 Å eliminates most of these features, confirming that they were caused by multiple scattering or backscattering from more distant atoms.

The peak amplitude of the 150ºC synthetic nontronite EXAFS spectrum was lower than those of the natural samples, indicating this sample was less crystalline. The second FT peak for nearest-neighbor cation backscattering was shifted to a slightly shorter distance, suggesting that the influence of the high Al content of this sample on average backscattering distances. The presence of

https://doi.org/10.1346/CCMN.2014.0620202 Published online by Cambridge University Press

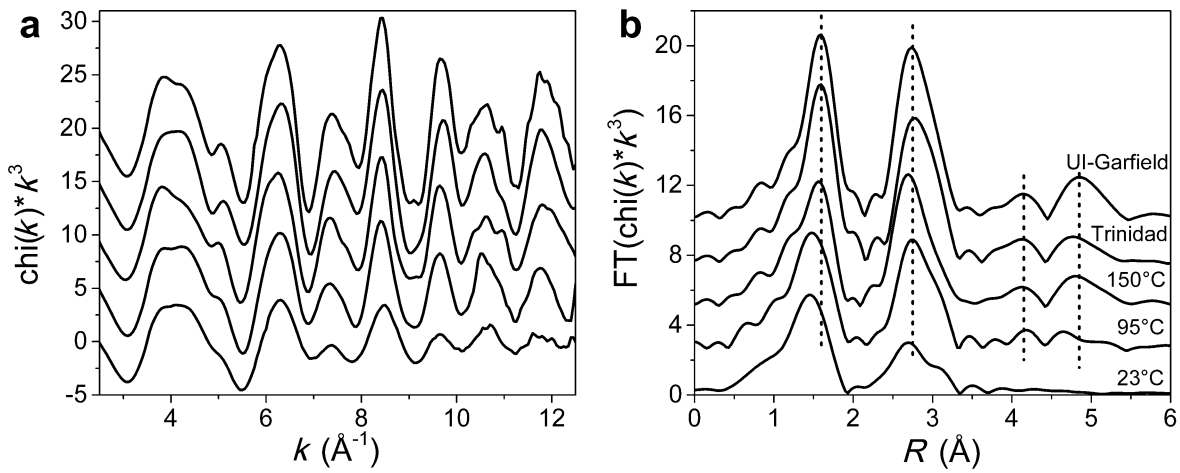

Figure 5. Chi spectra (a) and magnitude of Fourier transforms (b) of UI-Garfield and Trinidad nontronites, and synthetic nontronites crystallized at 23, 95, and 150ºC. The sample incubated at 4ºC is not shown, but is identical to that at 23ºC. Dashed lines in (b) at 1.6, 2.75, 4.15, and 4.85 Å are provided to compare relative peak positions between samples.

well developed FT peaks centered near 4.1 and 4.8 Å, resulting from backscattering by second-neighbor tetrahedral and octahedral cations, indicated that the 150ºC nontronite was well ordered to a distance of at least ~5.3 Å, the distance of the second octahedral neighboring cation in well ordered nontronite (Manceau *et al*., 1998).

The 95ºC synthetic nontronite spectrum had a lower EXAFS amplitude than either the 150ºC synthetic sample or the two natural nontronite spectra. Many of the fine-scale features associated with the second octahedral neighbor backscattering that were observed in the 150ºC and natural nontronite spectra were absent or poorly developed in the 95ºC nontronite. A small peak was present at 4.6 Å in the Fourier-transformed spectrum, suggesting that the 95ºC synthetic nontronite does not have a well ordered shell of second octahedral cation neighbors. Thus, well ordered domains in this sample appeared to be <5 Å in radius.

The 23ºC and 4ºC synthetic nontronites displayed little structure beyond the first octahedral cation backscattering shell at ~3 Å. The two samples were very similar to one another, and neither appeared to have developed structure beyond that of a gel precipitate, or possibly a hisingerite-like structure.

Shell fitting

Shell fitting was carried out on the synthetic and natural nontronites. The fitting results for the UI-Garfield nontronite spectrum have previously been described by Baker and Strawn (2012), and the methodology described in that paper was used for fitting the synthetic and natural nontronites. The well characterized Garfield nontronite has been modeled out to 6 Å (Manceau *et al.*, 1998). For the less crystalline nontronites examined in the present study, however, fitting of more distant backscatterers and multiple scattering paths was not feasible. Thus, fits in this study focused on contributions of single-scattering paths within 4 Å, and on the relative contributions of Fe and Al nearest-neighbor backscatterers.

Because all the synthetic samples had a bulk composition with Fe:Al = 1, any sample in which the octahedral cations were randomly arranged should have a 1:1 ratio, regardless of synthesis temperature. Cations in phyllosilicate octahedral sheets are frequently distributed non-randomly, however, forming small domains or clusters of Fe or Al. This study, therefore, fitted the number of Fe and Al nearest neighbors around the central Fe atom, constraining the sum to be three total nearest-neighbor octahedral cations. Although natural samples contain small amounts of Mg, concentrations of this element are much lower than Fe and Al concentrations (Table 1), and the synthetic samples were Mg-free, thus the fits did not include Mg.

Fitting of UI-Garfield nontronite using the 6-shell model produced results in agreement with those published by Baker and Strawn (2012) and by Manceau *et al.* (1998) (Figure 6 and Table 3). This high-Fe nontronite contained very little Al (Table 1) and the number of Fe-Al nearest neighbors fit to zero. In Trinidad nontronite (Figure 6), nearest-neighbor octahedral cations were dominated by Fe, with the Al:Fe ratio optimizing to 1:5 (Table 3). This ratio was very close to a previous estimate for SWa-1 made from EXAFS fitting (Vantelon *et al.*, 2003). The actual bulk molar Al:Fe ratio of Trinidad nontronite was ~1:3 (Table 1). Errors in fitting second-shell coordination numbers have been reported to be on the order of 20% for relatively simple structures (O'Day *et al.*, 1994) and up to 40% for structures with moderate isomorphic substitution (Scheidegger *et al.*, 1996). Applying a 20% error to the Fe cation content estimated for Trinidad nontronite results in the Al:Fe ratio ranging from 0 to 1:2, a range

https://doi.org/10.1346/CCMN.2014.0620202 Published online by Cambridge University Press

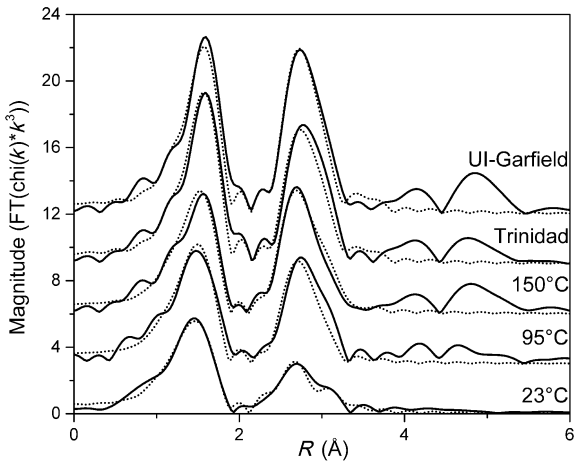

Figure 6. Shell fits to natural and synthetic nontronite samples using the parameters in Table 3.

that includes the fit results, but also suggests Fe could have a clustered distribution in this sample. The FTIR spectrum of the Trinidad nontronite also suggested it contained more Fe-Al nearest neighbors than UI-Garfield nontronite. The influence of Fe-Al backscattering was visible in the Fourier-transformed EXAFS spectrum of Trinidad nontronite as a slight broadening of the Fe-(Fe,Al) backscattering peak at 3 Å. The other fit parameters for Trinidad nontronite were similar to those fit for the UI-Garfield nontronite.

The 150ºC synthetic nontronite EXAFS (Figure 6) fit parameters were nearly identical to the theoretical path lengths for nontronite, and close to those optimized for the UI-Garfield standard (Table 3). The XRD data suggested that this sample had lower long-range crystallinity than the natural nontronites; the XAFS indicated that at the molecular scale, the structure was well ordered, however. The octahedral Fe-Fe and Fe-Al backscattering paths fit to identical distances. The *N*Fe value fitted to 2, suggesting an Al:Fe ratio of 1:2 in nearest-neighbor sites. This suggests some segregation of the octahedral cations into Fe-rich and Al-rich domains within the crystal. This observation is consistent with the observation of both Fe-Al-OH and Fe-Fe-OH features in its FTIR spectrum.

The 95ºC synthetic nontronite (Figure 6) XAFS fit values were also close to the UI-Garfield nontronite fit path lengths, with the exception of a shorter Fe–O1 path length (Table 3). The 0.02 Å difference in path length for the Fe–O1 path between the 95ºC and the 150ºC synthetic nontronites supports the XANES data interpretation that some tetrahedral Fe was present in the synthetic nontronite samples incubated at lower temperatures. The first-shell Debye-Waller parameter for the synthetic samples was greater than in the natural nontronites, which may be caused by both the tetrahedral Fe contribution and a more distorted first shell. The fitted Al:Fe ratio in the 95ºC sample (1.34:1.66) was greater than for the 150ºC sample, and was closer to the bulk composition of the sample, suggesting a random distribution of Fe and Al in the octahedral sheet.

The fit of the 23ºC synthetic nontronite (Figure 6) resulted in significant shortening of some backscattering paths compared to the higher-temperature synthetic samples, and the natural nontronites (Table 3). The fitted first shell Fe–O1 path length in the 23ºC synthetic nontronite was shorter than the 95ºC sample, and the Debye-Waller factor for that path was higher. The shorter distance and increased disorder for the first shell probably resulted from the presence of more tetrahedral Fe than was present in the higher-temperature nontronite samples. The fitted octahedral Al:Fe ratio was ~2:1, an interesting result in that it was greater than the bulk Al:Fe ratio. This may occur because of an ordered distribution of Fe within the octahedral sheet and may also be affected by the presence of tetrahedral Fe in the sample, particularly if Fe and Al do not partition equally into tetrahedral sites. Fe occupancies of up to 0.92 of 8 tetrahedral cations (11.5%) in natural nontronite samples were calculated by Gates *et al.* (2002) who observed that the sample with the greatest tetrahedral Fe content, NG-1, had a pre-edge peak height approximately twice that of Garfield nontronite. In the present study, the pre-edge peak height for the two lower-temperature nontronite samples was approximately twice that of UI-Garfield nontronite (Figure 7), suggesting a tetrahedral occupancy in the low-temperature nontronite gels of 10–20%.

DISCUSSION

Comparison of natural and synthetic nontronites

The results of XRD and FTIR analysis indicate that synthetic nontronites incubated for 4 weeks did not achieve the same degree of ordering as natural

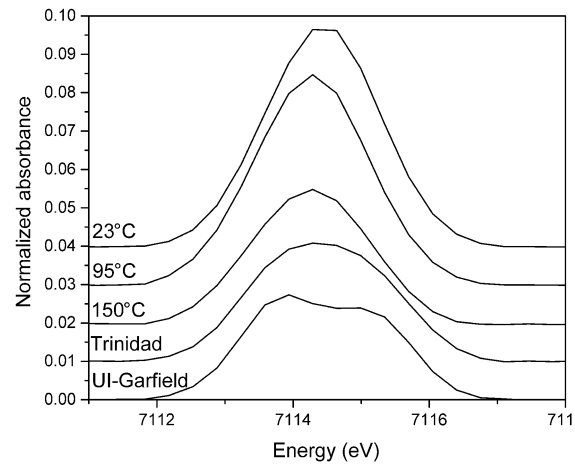

Figure 7. XANES pre-edge peaks (as in Figure 3 inset), with background slope subtracted for measurement of peak amplitudes. Each peak is offset vertically by 0.01 units for clarity, but relative amplitudes are correct.

https://doi.org/10.1346/CCMN.2014.0620202 Published online by Cambridge University Press

nontronite clays, even when incubated at 150ºC (Figures 1–2). On the local atomic scale, however, synthetic nontronite incubated at 150ºC for 4 weeks revealed a similar degree of ordering to natural UI-Garfield nontronite (Figures 3, 5). The synthetic nontronite incubated at 95ºC displayed some nontronite-like structure, detectable by FTIR and XAFS (Figures 2, 3, 5), but little longer-range ordering detectable by XRD (Figure 1). On the atomic scale, the 95ºC sample was clearly less well ordered than the natural nontronite samples or the 150ºC sample. An inflection in the XANES at 7132 eV (Figure 3) was observed in all the synthetic samples, but was only weakly developed in samples incubated at lower temperatures. Development of a strong inflection at this energy may result from the presence of well ordered backscattering shells within 4 Å of the target atom (Chen *et al.*, 2002). The well developed peaks at this energy in the two higher-temperature synthetic nontronites suggest that at the molecular scale, the atomic ordering was comparable to that in the natural nontronites.

The synthetic nontronite incubated at 23ºC did not display well formed nontronite structure, and its spectrum was identical to that of the precursor gel incubated at 4ºC (data not shown). This 23ºC nontronite was comparable in terms of atomic ordering to an Fe-substituted allophane gel or to hisingerite (Baker and Strawn, 2012). The XANES peak at 7132 eV (Figure 3) in the 23ºC sample was of comparable size to that in Fe-allophane, suggesting that the limit of the backscattering order was ~4 Å , and thus that coherent domains were <8 Å in diameter. The Fe-Fe peak at 3 Å in this sample was also very poorly developed compared to the higher-temperature samples (Figure 5), indicating a lack of ordering even within this distance of the central backscattering Fe atom. This suggested that well ordered domains within the 23ºC sample may be as small as 4–5 Å in diameter. Assuming this growth rate can be extrapolated meaningfully, coherent domains of ~100 Å in diameter would form in ~2 y. This result is reasonably consistent with the growth rates measured by Decarreau *et al.* (1987), who suggested coherent domains ~100 Å in diameter would form in ~10 y at 23ºC. Given the relatively poor constraints on both estimates, these results agree fairly well, and support the argument that, at ambient surface temperatures, formation of nontronite particles that approached macroscopic crystalline structure would require several years.

The formation temperature of natural nontronites in the CRB can be constrained based on field observations. Because liquid water is necessary for nontronite formation, basalt can be altered at >100ºC only under sufficient confining pressure to condense water. The nontronite localities in the CRB sampled in this study occurred in open cracks in basalt flows within a few meters of the surface, indicating that nontronite formation occurred at or near atmospheric pressure. At Garfield, Washington, for example, nontronite was found <1 m below the surface in vertical cracks open to the basalt flow surface. Thus, although nontronite formation at Garfield may have been accelerated by residual heat from emplacement of the host basalt, it cannot have occurred at temperatures above 100ºC because liquid water in the open cracks would have escaped by boiling. The Trinidad nontronite showed field evidence of having been influenced directly by heat from the emplaced basalt, and by water derived from the underlying paleosols, but it formed only a few meters below the surface and would not have been subject to significant confining pressure. Similar constraints are observed for other nontronite occurrences in the CRB (Baker *et al.*, 2012). Thus, these natural CRB nontronites are all likely to have formed at temperatures of <100ºC.

The synthetic nontronites included a sample incubated at 95ºC, close to the highest temperature likely for the natural nontronite formation conditions. This sample was considerably less ordered than the natural samples, however. Thus, the high degree of crystallinity observed in the natural nontronites is not due to crystallization at high temperatures, in agreement with the conclusions of Decarreau *et al.* (1987, 2008). The high crystallinity of naturally occurring nontronites suggests that these samples formed over long periods of time at ambient near-surface conditions. Variation in natural conditions, such as wetting-drying cycles and winter-summer temperature oscillations, may promote recrystallization of natural nontronites to more ordered forms.

Some nontronitic clays formed in basalts from Mururoa Atoll show textural evidence of having precipitated directly from boiling fluids shortly after basalt emplacement, with the fluids being derived either externally or from a residual magmatic phase (Meunier *et al.*, 2008, 2012). Based on the oxygen isotopic composition of the Mururoa nontronites (Meunier *et al.*, 2008), estimated formation temperatures were between 64 and 109ºC, although higher temperatures for void-filling clays that appeared to have formed by direct precipitation were suggested. The experimental work of Decarreau *et al.* (2008) places a high-temperature limit of 200ºC for the formation of the void-filling clays. No such textural evidence has been observed for CRB nontronites.

Constraining growth rates and conditions for natural nontronites

The UI-Garfield and Trinidad nontronites both occurred in flows of Wanapum age, ~14 m.y. (Swanson *et al.*, 1979) which represents the maximum possible formation time for the natural nontronite samples. This formation time would facilitate slow growth of nontronite, mostly at ambient surface temperatures. Previous studies have suggested that basalt alteration products typically formed at more elevated temperatures such as those measured by Meunier *et al.*

https://doi.org/10.1346/CCMN.2014.0620202 Published online by Cambridge University Press

(2008). The formation of palagonite and nontronite *vs*. temperature in a drill hole in basaltic lavas at Surtsey Volcano, Iceland, was calibrated by Jakobsson and Moore (1986) who found that at 100ºC palagonite formed a rim on basaltic glass at a rate of 2.8 μm/y, and that this rate doubled with every 12ºC increase in temperature. At temperatures >120ºC, nontronite formed a rim on olivine crystals at a rate of 0.3 μm/y; this rate doubled with every 8ºC increase, but nontronite growth was not observed at lower temperatures. This growth rate is faster than the rates measured experimentally by Decarreau *et al*. (1987), but drops more rapidly with temperature. A measurable thickness of palagonite was observed forming at Surtsey at ambient water temperatures of 7–10ºC. Palagonite has been shown to consist primarily of nontronite (Summers, 1976; Stroncik and Schmincke, 2002), but the fibropalagonite identified by Jakobsson and Moore (1986) at Surtsey is described as containing more TiO_2, Al_2O_3, and CaO, and less FeO, than nontronite samples collected from the same site. This growth rate is faster than the rates measured experimentally by Decarreau *et al.* (1987), but drops more rapidly with temperature.

The growth rates measured by Jakobsson and Moore (1986) may not be directly applicable to nontronites in the CRB. Olivine is rare in CRB, and nontronite in the basalts coats or fills glass rather than olivine crystals. In addition, the physical environment of CRB nontronites constrains their formation temperatures to be <100ºC. Calculations based on the published nontronite growth rates nonetheless provide some constraints on plausible formation times for CRB nontronites. Nontronites from Garfield, Washington, and at other CRB sites fill cracks up to 1 cm wide, although narrower cracks are more typical. Extrapolating the rate of nontronite formation from olivine at Surtsey at 120ºC (Jakobsson and Moore, 1986) down by a factor of two with every 8ºC decrease in temperature yields an estimate of the rate of nontronite formation at 95ºC of ~0.03 μm/y. Assuming a 1-cm wide crack is filled with pure nontronite that is growing as a rim on the basalt glass on both sides of the crack, formation of 1 cm nontronite veins in the CRB would take 1.67×10^5 y. Palagonite at Surtsey grew at a rate of 2.8 μm/y at 100ºC (Jakobsson and Moore, 1986), and even at this faster growth rate, ~1800 y would be required for a 1 cm crack to fill with palagonite.

In the absence of other heat sources, nontronite growth rates may also be constrained by considering basalt cooling rates. For a CRB nontronite precipitated in an open crack, the temperature of formation must have been below the boiling point of water. Detailed models of basalt cooling suggest that the material within 1 m of a basalt flow surface will take a period of several years to cool from 100ºC to ambient temperatures (Lore *et al.*, 2000). Studies of field constraints on emplacement and cooling of individual Columbia River Basalt flows (Long and Wood, 1986; Reidel, 1998; Thordarson and Self, 1998) estimate cooling timescales on the order of several years, although these studies focus more on cooling to solidification rather than to ambient temperature. If CRB nontronite formation occurred at temperatures close to 100ºC after basalt emplacement and solidification, formation rates would have to be several orders of magnitude higher than those observed by Jakobsson and Moore (1986) to account for the nontronite occurrences observed in the weathered CRB.

If nontronite were to form *via* basalt alteration at high temperatures, then rapid cooling of basalt flows requires that this process occur within a period of years to hundreds of years, more rapidly than has been observed in the studies cited above. Otherwise nontronite formation must continue after the flow has cooled to ambient conditions. Given that reaction kinetics are strongly temperature-dependent, nontronite crystallization at ambient conditions is expected to be a slow process. Extrapolating the measured growth rates of Jakobsson and Moore (1986) down to an ambient temperature of 20ºC suggests a rate of <1 nm/y, fairly comparable to the estimate above for the synthetic sample incubated at 23ºC. This implies formation times on the order of millions of years to develop 1 cm of crack-filling nontronite, suggesting that nontronite formation has been ongoing for much or all of the 14 million y since emplacement of the hosting basalts. Diurnal heating of the host basalts may have accelerated nontronite growth rates somewhat; near-surface temperatures of up to 65ºC have been measured on basalt flows at Craters of the Moon National Monument, Idaho, USA (Day and Wright, 1989).

If nontronite continues to crystallize at ambient surface temperatures, then natural nontronite occurrences would be expected to include samples with a wide range of crystallinity, representing different total times of crystallization and resembling the range of crystallinity observed in the synthetic samples. Clay infill in cracks and void spaces might be predicted in this case to exhibit zoned crystallinity, but this has not been described in CRB. Collection of such samples would represent evidence that nontronite formation is an ongoing process in CRB weathering.

Nontronite has been observed in very old (>3.5 Ga) rocks on Mars by orbiting spacecraft, and this observation has been presented as evidence for water–rock interaction in the ancient Martian past (Bishop *et al.*, 2008; Ehlmann *et al.*, 2011). The presence of this and other clay minerals on Mars may provide information about the Martian climate and hydrosphere at the time of clay formation. As the results of the present study suggest nontronite formation is relatively slow, this suggests relatively long periods of water–rock interaction on Mars. Further information on nontronite-formation conditions on Earth, and on the characteristics of the Martian nontronite occurrences, will help to refine this conclusion.

https://doi.org/10.1346/CCMN.2014.0620202 Published online by Cambridge University Press

CONCLUSIONS

Synthetic nontronites incubated for 4 weeks at temperatures up to 150ºC did not achieve the degree of crystallinity observed in natural nontronite samples formed by weathering of Columbia River Basalts. Synthetic nontronites also exhibited lower degrees of cation ordering, and contained more tetrahedral Fe than natural samples. Because previously published studies indicate that nontronite does not form at temperatures >200ºC, this suggests that the formation of well ordered nontronite crystals requires much longer formation times than were used in this experimental study.

Field relations indicate that some Columbia River Basalt nontronites exhibiting good crystalline ordering must have formed at temperatures below the boiling point of water at the Earth's surface. Published estimates of nontronite growth rates suggest very slow growth at low temperature, a result in agreement with the present observations. Estimates of experimental nontronite crystallization rates, coupled with field constraints and published growth-rate estimates, suggest that naturally occurring CRB nontronites formed slowly over millions of years at ambient surface temperatures.

ACKNOWLEDGMENTS

The authors thank Jeff Boyle and Jim Harsh at Washington State University for locating and sharing field notes of J.A. Kittrick indicating the SWa-1 sample-collection locality. Ryan Nickerson assisted with sample synthesis and preparation and with XAFS analyses. Comments from two anonymous reviewers were helpful in improving the manuscript. Partial funding for this project was provided by an Idaho Space Grant Consortium Research Initiation Grant. Portions of this research were carried out at the Stanford Synchrotron Radiation Lightsource, a Directorate of SLAC National Accelerator Laboratory and an Office of Science User Facility operated for the U.S. Department of Energy Office of Science by Stanford University. The SSRL Structural Molecular Biology Program is supported by the DOE Office of Biological and Environmental Research, and by the National Institutes of Health, National Institute of General Medical Sciences (including P41GM103393). The contents of this publication are solely the responsibility of the authors and do not necessarily represent the official views of NIGMS or NIH.

REFERENCES

Allen, V.T. and Scheid, V.E. (1946) Nontronite in the Columbia River region. *American Mineralogist*, **31**, 294–312.

Baker, L.L. and Strawn, D.G. (2012) Fe K-edge XAFS spectra of phyllosilicates of varying crystallinity. *Physics and Chemistry of Minerals* **39**, 675–684.

Baker, L.L., Strawn, D.G., Vaughan, K.L., and McDaniel, P.A. (2010) XAS study of Fe mineralogy in a chronosequence of soil clays formed in basaltic cinders. *Clays and Clay Minerals* **58**, 6, 772–782.

Baker, L., Strawn, D., McDaniel, P., Fairley, J., and Bishop, J. (2012) Hydrologic and geochemical controls on nontronite formation in terrestrial Columbia River Basalts and implications for clay formation on Mars. *LPI Contributions* **1680**, 7011.

Benson, L.V. and Teague, L.S. (1982) Diagenesis of basalts from the Pasco Basin, Washington: I. Distribution and composition of secondary mineral phases. *Journal of Sedimentary Research*, **52**, 595–613.

Bishop, J.L., Dobrea, E.Z.N., McKeown, N.K., Parente, M., Ehlmann, B.L., Michalski, J.R., Milliken, R.E., Poulet, F., Swayze, G.A., Mustard, J.F., Murchie, S.L., and Bibring, J.-P. (2008) Phyllosilicate diversity and past aqueous activity revealed at Mawrth Vallis, Mars. *Science*, **321**, 830–833.

Chen, L.X., Liu, T., Thurnauer, M.C., Csencsits, R., and Rajh, T. (2002) Fe_2O_3 nanoparticle structures investigated by X-ray absorption near-edge structure, surface modifications, and model calculations. *The Journal of Physical Chemistry B*, **106**, 34, 8539–8546.

Cole, T. and Shaw, H. (1983) The nature and origin of authigenic smectites in some recent marine sediments. *Clay Minerals* **18**, 3, 239–252.

Day, T.A. and Wright, R.G. (1989) Positive plant spatial association with Eriogonum ovalifolium in primary succession on cinder cones: seed-trapping nurse plants. *Plant Ecology*, **80**, 37–45.

Decarreau, A. and Bonnin, D. (1986) Synthesis and crystallogenesis at low temperature of Fe (III)-smectites by evolution of coprecipitated gels: experiments in partially reducing conditions. *Clay Minerals*, **21**, 861–877.

Decarreau, A., Bonnin, D., Badaut-Trauth, D., Couty, R., and Kaiser, P. (1987) Synthesis and crystallogenesis of ferric smectite by evolution of Si-Fe coprecipitates in oxidizing conditions. *Clay Minerals*, **22**, 207–223.

Decarreau, A., Petit, S., Martin, F., Farges, F., Vieillard, P., and Joussein, E. (2008) Hydrothermal synthesis, between 75 and 150ºC, of high-charge, ferric nontronites. *Clays and Clay Minerals* **56**, 322–337.

Dekov, V.M., Kamenov, G.D., Stummeyer, J., Thiry, M., Savelli, C., Shanks, W.C., Fortin, D., Kuzmann, E., and Vértes, A. (2007) Hydrothermal nontronite formation at Eolo seamount (Aeolian volcanic arc, Tyrrhenian Sea). *Chemical Geology*, **245**, 103–119.

Eggleton, R. (1977) Nontronite: Chemistry and diffraction. *Clay Minerals*, **12**, 181–194.

Ehlmann, B.L., Mustard, J.F., Murchie, S.L., Bibring, J.-P., Meunier, A., Fraeman, A.A., and Langevin, Y. (2011) Subsurface water and clay mineral formation during the early history of Mars. *Nature*, **479**, 7371, 53–60.

Farmer, V., Krishnamurti, G., and Huang, P. (1991) Synthetic allophane and layer-silicate formation in SiO_2-Al_2O_3-FeO-Fe_2O_3-MgO-H_2O systems at 23ºC and 89ºC in a calcareous environment. *Clays and Clay Minerals*, **39**, 561–570.

Farmer, V., McHardy, W., Elsass, F., and Robert, M. (1994) hk-ordering in aluminous nontronite and saponite synthesized near 90ºC: Effects of synthesis conditions on nontronite composition and ordering. *Clays and Clay Minerals*, **42**, 180–180.

Fialips, C.-I., Huo, D., Yan, L., Wu, J., and Stucki, J.W. (2002) Effect of Fe oxidation state on the IR spectra of Garfield nontronite. *American Mineralogist*, **87**, 630–641.

Frost, R.L., Kloprogge, J.T., and Ding, Z. (2002) The Garfield and Uley nontronites – an infrared spectroscopic comparison. *Spectrochimica Acta Part A: Molecular and Biomolecular Spectroscopy*, **58**, 9, 1881–1894.

Gates, W.P. (2005) Infrared spectroscopy and the chemistry of dioctahedral smectites. Pp. 125–168 in: *Vibrational Spectroscopy of Layer Silicates and Hydroxides* (T. Kloprogge, editor). The Clay Minerals Society, Aurora, CO, USA.

Gates, W.P. (2008) Cation mass-valence sum (CM-VS) approach to assigning OH-bending bands in dioctahedral smectite. *Clays and Clay Minerals*, **56**, 10–22.

Gates, W.P., Slade, P.G., Manceau, A., and Lanson, B. (2002) Site occupancies by iron in nontronites. *Clays and Clay Minerals*, **50**, 223–239.

Harder, H. (1976) Nontronite synthesis at low temperatures. *Chemical Geology*, **18**, 169–180.

Harder, H. (1978) Synthesis of iron layer silicate minerals under natural conditions. *Clays and Clay Minerals*, **26**, 65–72.

Jakobsson, S.P. and Moore, J.G. (1986) Hydrothermal minerals and alteration rates at Surtsey volcano, Iceland. *Geological Society of America Bulletin*, **97**, 648–659.

Keeling, J.L., Raven, M.D., and Gates, W.P. (2000) Geology and characterization of two hydrothermal nontronites from weathered metamorphic rocks at the Uley graphite mine, South Australia. *Clays and Clay Minerals*, **48**, 5, 537–548.

Kerr, P.F. and Kulp, J.L. (1949) Reference clay localities, United States. Pp. 69–73 in: *Reference Clay Minerals;* American Petroleum Institute Research Project **49**, Preliminary Reports no. 1–8 (P.F. Kerr and J.L. Kulp, editors). Columbia University, New York.

Köhler, B., Singer, A., and Stoffers, P. (1994) Biogenic nontronite from marine white smoker chimneys. *Clays and Clay Minerals*, **42**, 689–701.

Long, P.E. and Wood, B.J. (1986) Structures, textures, and cooling histories of Columbia River basalt flows. *Geological Society of America Bulletin*, **97**, 1144–1155.

Lore, J., Gao, H., and Aydin, A. (2000) Viscoelastic thermal stress in cooling basalt flows. *Journal of Geophysical Research: Solid Earth (1978–2012)*, **105**, B10, 23695–23709.

Manceau, A., Bonnin, D., Stone, W.E.E., and Sanz, J. (1990) Distribution of Fe in the octahedral sheet of trioctahedral micas by polarized EXAFS; comparison with NMR results. *Physics and Chemistry of Minerals*, **17**, 363–370.

Manceau, A., Chateigner, D., and Gates, W.P. (1998) Polarized EXAFS, distance-valence least-squares modeling (DVLS), and quantitative texture analysis approaches to the structural refinement of Garfield nontronite. *Physics and Chemistry of Minerals*, **25**, 347–365.

Meunier, A., Mas, A., Beaufort, D., Patrier, P., and Dudoignon, P. (2008) Clay minerals in basalt-hawaiite rocks from Mururoa atoll (French Polynesia). II. Petrography and geochemistry. *Clays and Clay Minerals*, **56**, 730–750.

Meunier, A., Petit, S., Ehlmann, B.L., Dudoignon, P., Westall, F., Mas, A., El Albani, A., and Ferrage, E. (2012) Magmatic precipitation as a possible origin of Noachian clays on Mars. *Nature Geoscience*, **5**, 739–743.

Montarges-Pelletier, E., Bogenez, S., Pelletier, M., Razafitianamaharavo, A., Ghanbaja, J., Lartiges, B., and Michot, L. (2005) Synthetic allophane-like particles: textural properties. *Colloids and Surfaces A: Physicochemical and Engineering Aspects*, **255**, 1–10.

Neumann, A., Petit, S., and Hofstetter, T.B. (2011) Evaluation of redox-active iron sites in smectites using middle and near infrared spectroscopy. *Geochimica et Cosmochimica Acta*, **75**, 2336–2355.

O'Day, P.A., Rehr, J.J., Zabinsky, S.I., and Brown, G.E., Jr. (1994) Extended X-ray absorption fine structure (EXAFS) analysis of disorder and multiple-scattering in complex crystalline solids. *Journal of the American Chemical Society*, **116**, 2938–2949.

Ravel, B. and Newville, M. (2005) ATHENA, ARTEMIS, HEPHAESTUS: data analysis for X-ray absorption spectroscopy using IFEFFIT. *Journal of Synchrotron Radiation*, **12**, 537–541.

Reidel, S.P. (1998) Emplacement of Columbia River flood basalt. *Journal of Geophysical Research: Solid Earth (1978–2012)*, **103**, 27393–27410.

Reidel, S.P., Camp, V.E., Tolan, T.L., and Martin, B.S. (2013) The Columbia River flood basalt province: Stratigraphy, areal extent, volume, and physical volcanology. *Geological Society of America Special Papers*, **497**, 1–43.

Russell, J.D. and Fraser, A.R. (1994) Infrared Methods. Pp. 11–67 in: *Clay Mineralogy: Spectroscopic and Chemical Determinative Methods* (M.J. Wilson, editor). Chapman & Hall, London.

Scheidegger, A.M., Lamble, G.M., and Sparks, D.L. (1996) Investigation of Ni sorption on pyrophyllite: An XAFS study. *Environmental Science & Technology*, **30**, 548–554.

Severmann, S., Mills, R.A., Palmer, M.R., and Fallick, A.E. (2004) The origin of clay minerals in active and relict hydrothermal deposits. *Geochimica et Cosmochimica Acta*, **68**, 73–88.

Shoji, S., Nanzyo, M., and Dahlgren, R. (1993) *Volcanic Ash Soils: Genesis, Properties and Utilization.* Elsevier, New York.

Stroncik, N.A. and Schmincke, H.U. (2002) Palagonite – a review. *International Journal of Earth Sciences*, **91**, 680–697.

Summers, K. (1976) The clay component of the Columbia River palagonites. *American Mineralogist*, **61**, 492–494.

Swanson, D.A., Wright, T.L., Hooper, P.R., and Bentley, R.D. (1979) *Revisions in Stratigraphic Nomenclature of the Columbia River Basalt Group: U.S. Geological Survey Bulletin no. 1457*. U.S. Government Printing Office.

Thordarson, T. and Self, S. (1998) The Roza Member, Columbia River Basalt Group: A gigantic pahoehoe lava flow field formed by endogenous processes? *Journal of Geophysical Research*, **103**, 27411–27427, 27445.

Ueshima, M. and Tazaki, K. (2001) Possible role of microbial polysaccharides in nontronite formation. *Clays and Clay Minerals*, **49**, 292–299.

Vantelon, D., Montarges-Pelletier, E., Michot, L.J., Pelletier, M., Thomas, F., and Briois, V. (2003) Iron distribution in the octahedral sheet of dioctahedral smectites. An Fe K-edge X-ray absorption spectroscopy study. *Physics and Chemistry of Minerals*, **30**, 44–53.

Webb, S.M. (2005) Sixpack: A graphical user interface for XAS analysis using IFEFFIT. *Physica Scripta*, **T115**, 1011–1014.

Westre, T.E., Kennepohl, P., DeWitt, J.G., Hedman, B., Hodgson, K.O., and Solomon, E.I. (1997) A multiplet analysis of Fe K-edge 1s → 3d pre-edge features of iron complexes. *Journal of the American Chemical Society*, **119**, 6297–6314.

(*Received 27 February 2014; revised 26 May 2014; Ms. 853; AE: R. Kukkadapu*)